

Strain, doping and electronic transport of large area monolayer MoS₂ exfoliated on gold and transferred to an insulating substrate

S.E. Panasci^{1,2}, E. Schilirò¹, G. Greco¹, M. Cannas³, F. M. Gelardi³, S. Agnello^{3,1,4}, F. Roccaforte¹,
F. Giannazzo^{1*}

¹ *CNR-IMM, Strada VIII, 5 95121, Catania, Italy*

² *Department of Physics and Astronomy, University of Catania, Via Santa Sofia 64, 95123 Catania, Italy*

³ *Department of Physics and Chemistry Emilio Segrè, University of Palermo, Via Archirafi 36, 90123 Palermo, Italy*

⁴ *ATeN Center, Università degli Studi di Palermo, Viale delle Scienze, Edificio 18, 90128 Palermo, Italy*

*E-mail: filippo.giannazzo@imm.cnr.it

Abstract

Gold-assisted mechanical exfoliation currently represents a promising method to separate ultra-large (cm-scale) transition metal dichalcogenides (TMDs) monolayers (1L) with excellent electronic and optical properties from the parent van der Waals (vdW) crystals. The strong interaction between Au and chalcogen atoms is the key to achieve this nearly perfect 1L exfoliation yield. On the other hand, it may affect significantly the doping and strain of 1L TMDs in contact with Au. In this paper, we systematically investigated the morphology, strain, doping, and electrical properties of large area 1L MoS₂ exfoliated on ultra-flat Au films (0.16-0.21 nm roughness) and finally transferred to an insulating Al₂O₃ substrate. Raman mapping and correlative analysis of the E['] and A₁' peaks positions revealed a moderate tensile strain ($\epsilon \approx 0.2\%$) and p-type doping ($n \approx 0.25 \times 10^{13} \text{ cm}^{-2}$) of 1L MoS₂ in contact with Au. Nanoscale resolution current mapping and current-voltage (I-V) measurements by conductive atomic force microscopy (C-AFM) showed direct tunnelling across the 1L MoS₂ on Au, with a broad distribution of tunnelling barrier values (Φ_B from 0.7 to 1.7 eV) consistent with the p-

type doping of MoS₂. After the final transfer of 1L MoS₂ on Al₂O₃/Si, the strain was converted to compressive ($\epsilon \approx -0.25\%$). Furthermore, an n-type doping ($n \approx 0.5 \times 10^{13} \text{ cm}^{-2}$) was deduced by Raman mapping and confirmed by electrical measurements of an Al₂O₃/Si back-gated 1L MoS₂ transistor. These results provide a deeper understanding of the Au-assisted exfoliation mechanisms and can contribute to its widespread applications for the realization of novel devices and artificial vdW heterostructures.

1. Introduction

Semiconducting transition metal dichalcogenides (TMDs) are a class of two-dimensional (2D) layered materials with the general chemical formula MX₂, being M a transition metal (Mo, W,...) and X a chalcogen (S, Se,...), which are characterized by strong (covalent) in plane bonds and weak Van der Waals (vdW) interactions between the layers [1]. In particular, due to its abundance in nature and good stability under ambient conditions, molybdenum disulphide (MoS₂) has been the most widely investigated TMD for potential applications in electronics, optoelectronics, photodetection and sensing [2,3,4,5]. In its bulk form, MoS₂ shows an indirect band gap of 1.2 eV, whereas the monolayer counterpart exhibits a direct band gap of ~1.8 eV [6,7,8,9,10]. The sizeable bandgap, combined with a low dielectric constant, made MoS₂ a potential candidate to replace silicon as channel material in ultra-thin body field effect transistors for next generation CMOS applications [11,12,13]. Furthermore, bandgap tunability of MoS₂, obtained by tailoring the number of layers [14], strain [15] or dielectric environment [16], offers many possibilities to realize new concept beyond-CMOS electronic devices [17].

Many of the MoS₂ device prototypes demonstrated so far have been fabricated using monolayer or few layer flakes obtained by mechanical exfoliation from bulk molybdenite. In spite of the reported progresses in the large area synthesis of TMDs by scalable deposition techniques (including chemical vapour deposition [18,19], molecular beam epitaxy [20] and pulsed laser deposition [21]), mechanical exfoliation still remains a method of choice for investigating basic physical phenomena and to demonstrate new device concepts, due to the superior quality of the material produced by this approach [22,23].

To overcome the limitations represented by the small (micrometer) size of the exfoliated flakes and the lack of reproducibility in the thickness, appropriate strategies allowing to increase the exfoliated monolayer area have been recently elaborated. In particular, the so-called “gold-assisted” mechanical exfoliation approach showed the possibility of separating large area (cm²) monolayer MoS₂ (1L

MoS₂) from a bulk crystal stamp by exploiting the strong affinity between a gold film and the topmost sulphur atoms of MoS₂ [24,25,26,27]. The Au/1L MoS₂ stack can be also transferred to insulating substrates and, after Au removal by chemical etching, the large area MoS₂ film exhibits electronic properties fully comparable with those of the semiconducting MoS₂ flakes obtained by the conventional Scotch tape exfoliation [25,28]. The gold-assisted exfoliation approach has been shown to be effective also with other common TMDs (such as MoSe₂, WS₂, WSe₂, MoTe₂, WTe₂, and GaSe) [24,26,29] and it has been recently proposed as a general approach to produce large area heterostructures of different TMDs with outstanding electronic quality by sequentially stacking the exfoliated monolayers [29].

In the last few years, several morphological and spectroscopic investigations have been reported on the Au/MoS₂ system, with the aim of deeply understanding the mechanisms of the Au-assisted exfoliation and to maximize the monolayer fraction and the lateral size of the obtained MoS₂ films. In particular, the 1L exfoliation yield was shown to be strongly influenced by the gold surface morphology and its exposure to the air before exfoliation [24]. Due to the strong vdW interaction at MoS₂/Au interface, the Au morphology may significantly affect also the doping and strain in 1L MoS₂, as shown by Raman analyses [27]. An increase of the density of states (DOS) at the Fermi energy (i.e. a metallic character) was predicted by ab-initio simulations of the MoS₂/Au heterostructure as compared to semiconducting free-standing MoS₂ [24]. Such increased DOS in 1L MoS₂ associated to the underlying Au was also demonstrated by electrochemical characterization of the MoS₂/Au system [24].

In this context, a systematic study on the evolution of the structural and electronic properties of 1L MoS₂ in the different stages of the Au-assisted exfoliation process, i.e. after adhesion with gold and after final transfer to an insulating substrate, would be highly desirable.

In this work, we investigated the morphology, strain, doping, and electrical properties of 1L MoS₂ exfoliated on ultra-flat Au films and finally transferred to an Al₂O₃/Si substrate. The correlative analysis of the E' and A₁' Raman peaks positions in spatial mapping revealed a moderate tensile strain (~0.2%) and p-type doping ($0.25 \times 10^{13} \text{ cm}^{-2}$) of 1L MoS₂ in contact with Au. Nanoscale resolution current mapping and current-voltage (I-V) measurements by conductive atomic force microscopy (C-AFM) showed direct tunnelling across the 1L MoS₂ on Au, with a broad distribution of tunnelling barrier values (Φ_B from 0.7 to 1.7 eV) indicating wide point to point variations of MoS₂ p-type doping. After the final transfer of 1L MoS₂ on Al₂O₃/Si and complete removal of the Au film, the strain was converted to compressive (-0.25%) and a n-type doping of $\sim 0.5 \times 10^{13} \text{ cm}^{-2}$ was observed

both by Raman and confirmed by electrical measurements on a Al₂O₃/Si back-gated 1L MoS₂ transistor.

2. Results and discussion

The lateral extension and thickness uniformity of MoS₂ monolayers exfoliated on a smooth gold surface was initially assessed. To this aim, a 15 nm thick Au film was deposited onto a SiO₂/Si substrate by DC magnetron sputtering (as schematically reported in Fig.S1). Prior to Au deposition, a 10 nm thick Ni film was sputtered to improve the adhesion onto the SiO₂. Beside ensuring an optimal adhesion to the SiO₂ surface, the Ni interlayer was beneficial to achieve a very smooth surface of the Au overlayer, with a low root-mean-square (RMS) roughness of 0.16 nm, as deduced from the tapping mode atomic force microscopy (AFM) image reported in Fig.S2 of Supporting Information. Mechanical exfoliation of MoS₂ was carried out on the fresh Au surface, i.e. immediately after the deposition, in order to avoid its contamination with adventitious carbon, which is known to reduce the interaction strength between S atoms and Au [24]. By this procedure, very large area MoS₂ films, mostly composed of monolayer, were separated from the bulk crystal.

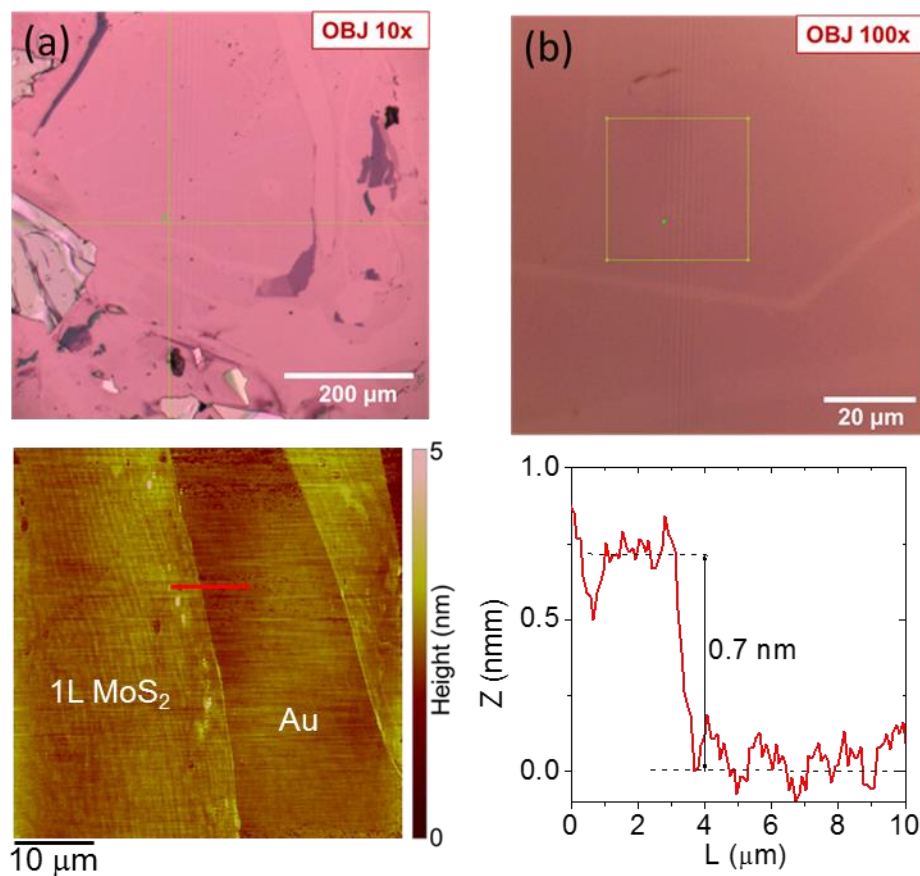


Fig.1 (a,b) Optical images at two different magnifications, 10× and 100×, of the exfoliated MoS₂ on the Au/Ni/SiO₂. (c) AFM image of the ultra-thin MoS₂ film with a fracture and (d) height profile along the dashed red line. The step height of ~0.7 nm demonstrates the 1L thickness of MoS₂.

Fig.1(a) and (b) show two optical images at different magnifications (10× and 100×, respectively) of the exfoliated MoS₂ on the Au surface. The presence of an ultra-thin MoS₂ film extending for several hundreds of micrometres can be deduced from the colour contrast in the lower magnification image (Fig.1(a)), which also shows the presence of thicker MoS₂ areas with smaller size, and of fractures of the MoS₂ membrane (i.e. bare Au regions) due to the exfoliation process. The optical contrast difference between the uniform ultra-thin MoS₂ membrane and one of these fractures can be better visualized in the higher magnification image in Fig.1(b). Furthermore, a typical tapping mode AFM image of a fracture of the MoS₂ film is reported in Fig.1(c). The ~0.7 nm step height measured by the line profile in Fig.1(d) is a direct confirmation of the 1L thickness of the MoS₂ membrane.

After assessing the thickness uniformity of 1L MoS₂ films exfoliated on gold, we investigated the transfer of these films to an insulating substrate, which is a mandatory requirement for most of electronic applications. More specifically, a Si substrate covered by 100 nm Al₂O₃ film was employed in this experiment, although the transfer procedure can be easily extended to other semiconductors or dielectric materials. Following the approach recently demonstrated by *Liu et al.* [29], the transfer procedure consisted of three different steps, schematically illustrated in Fig.2. The first step was the fabrication of an ultra-flat “gold tape”, consisting of a gold film on a polymer substrate. To this aim, a ~100 nm thick Au layer was deposited by DC magnetron sputtering on an accurately pre-cleaned silicon sample. Afterwards, the Au surface was spin-coated by a protective PMMA layer and attached to a thermal release tape (TRT). By exploiting the poor adhesion between Au and Si, the TRT/PMMA/Au stack was easily peeled from the silicon surface, thus obtaining the desired “gold tape”. The surface of Au films prepared by this method is typically very flat [30,31] and it has been already demonstrated to be suitable for the exfoliation of large area monolayers of MoS₂ and other TMDs [29]. In particular a RMS roughness of 0.21 nm was evaluated by AFM on the peeled Au films on PMMA in our experiments (see Fig.S3 of Supporting Information), which is comparable with that of the Au/Ni film on SiO₂.

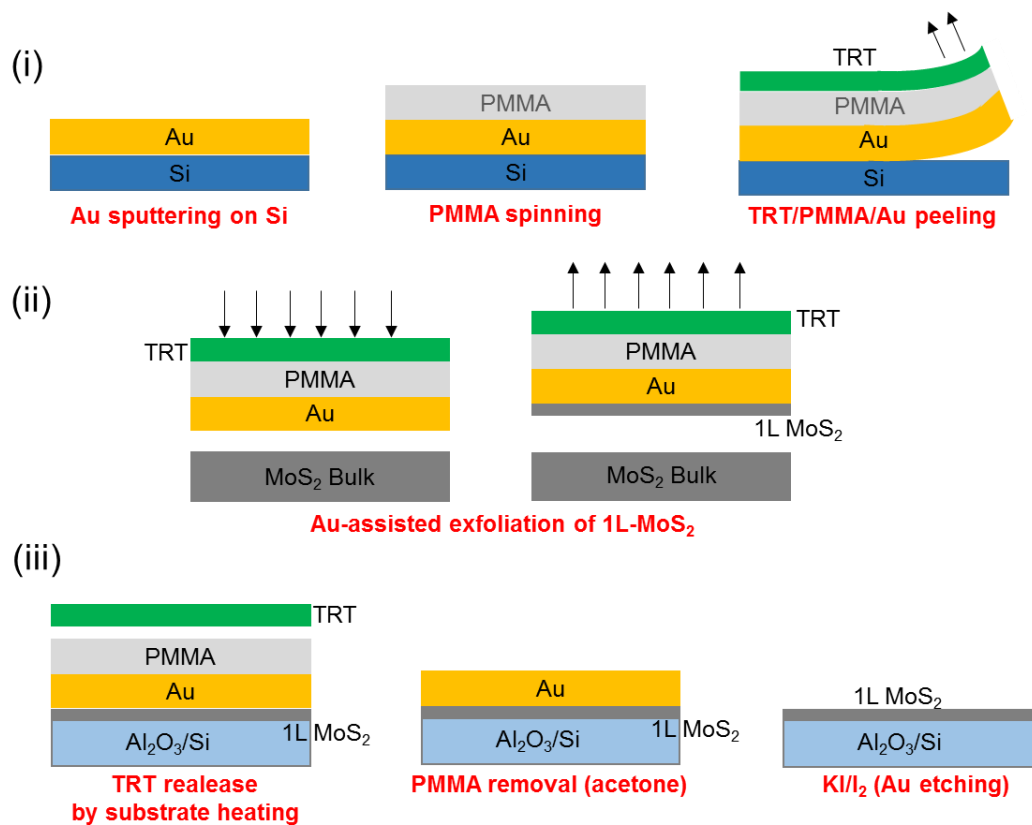


Fig.2 Schematic illustration of the three steps for Au-assisted exfoliation of 1L MoS₂ and transfer to a Al₂O₃/Si substrate: (i) preparation of a gold tape on PMMA; (ii) 1L MoS₂ exfoliation from bulk; (iii) transfer to the final substrate.

The TRT/PMMA/Au stamp with a fresh Au surface, i.e. immediately after peeling from Si, was used to exfoliate 1L MoS₂ from a MoS₂ bulk sample. The final step of the process was the transfer of 1L MoS₂ on the target Al₂O₃/Si surface. This was achieved by pressing the TRT/PMMA/Au/1L MoS₂ stack onto the Al₂O₃/Si substrate while heating at 120 °C to promote the TRT release, followed by PMMA removal and final chemical etching of the Au film (with KI/I₂ solution).

Fig.3(a) reports a typical optical microscopy image of the transferred MoS₂ membrane on the Al₂O₃ surface. As compared to the case of 1L MoS₂ exfoliated on gold (Fig.1(a) and (b)), a much sharper colour contrast can be observed between the regions coated by the extended 1L MoS₂ membrane (blue) and bare Al₂O₃ regions (violet), due to the favourable optical interference with the 100 nm Al₂O₃/Si substrate. Furthermore, the small size regions coated by few-layer or multilayer MoS₂ can be easily identified by the azure or bright colour, respectively. Hence, the optical image provides useful information on the thickness uniformity of the transferred MoS₂ film on large area. Furthermore, a morphological AFM image of a sample region partially covered by the MoS₂ membrane is shown in Fig.3(b). The monolayer MoS₂ thickness is directly confirmed by the ~0.7 nm step height measured by the linescan in Fig.3(c).

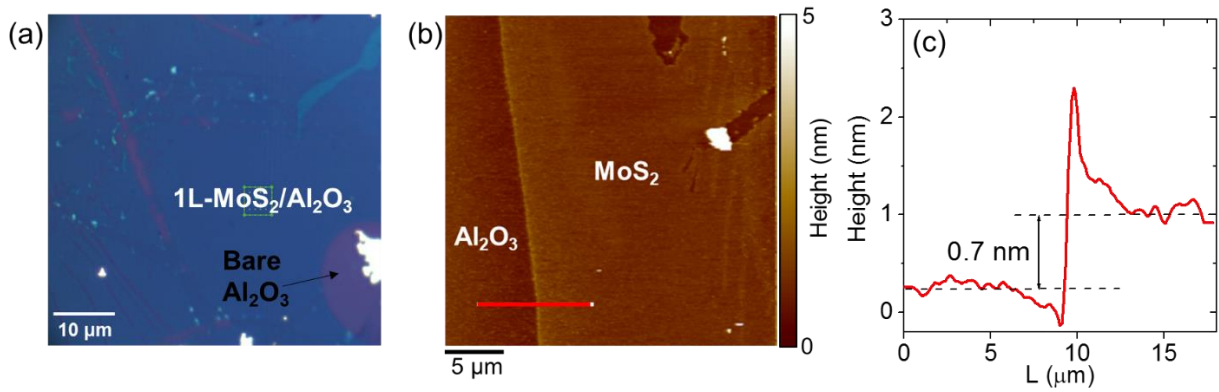


Fig.3 (a) Optical image ($50\ \mu\text{m}\times 50\ \mu\text{m}$) and (b) AFM morphology on large area ($25\ \mu\text{m}\times 25\ \mu\text{m}$) of the transferred 1L MoS₂ membrane on the Al₂O₃/Si substrate. (c) Height line-scan confirming the monolayer thickness.

The large area 1L MoS₂ membranes exfoliated on Au and transferred onto Al₂O₃/Si were extensively investigated by micro-Raman mapping and photoluminescence (PL) spectroscopy, in order to evaluate the impact of the different substrates on relevant parameters, such as the doping and strain distribution.

Fig.4(a) shows the comparison between two representative Raman spectra for 1L MoS₂ on Au (black line) and on Al₂O₃/Si (red line), with indicated the characteristic E' and A₁' peaks, associated to the in-plane and out-of-plane MoS₂ vibrational modes, respectively. Noteworthy, a peaks frequency difference $\Delta\omega=18\ \text{cm}^{-1}$ is measured for our large-area 1L MoS₂ produced by Au-assisted exfoliation and transferred onto Al₂O₃, a value very similar to those reported for mechanically exfoliated or CVD grown 1L MoS₂ on common insulating substrates (such as SiO₂) [23,32]. On the other hand, for the Au-supported 1L MoS₂, the E' peak exhibits a red-shift and the A₁' peak a blue-shift, resulting in a significantly larger $\Delta\omega=21\ \text{cm}^{-1}$. It is well known that E' and A₁' spectral features are highly sensitive to strain and doping of 1L MoS₂ [33,34]. In particular, a red shift of E' peak is typically observed with increasing the tensile strain [35,36], followed by a peak splitting for large strain values [27,37]. On the other hand, the A₁' peak is known to be sensitive to doping, and a blue (red) shift of its position is typically reported for p-type (n-type) doping of 1L MoS₂ [38]. Hence, the increase of $\Delta\omega$ for 1L MoS₂ on Au/Ni/SiO₂/Si can be ascribed to a change both in the strain and doping of the 2D membrane.

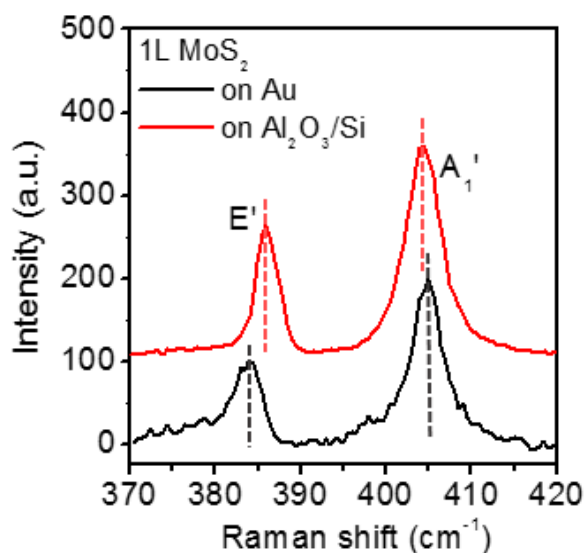


Fig.4 (a) Representative Raman spectra for 1L MoS₂ on Au (black line) and on Al₂O₃/Si (red line).

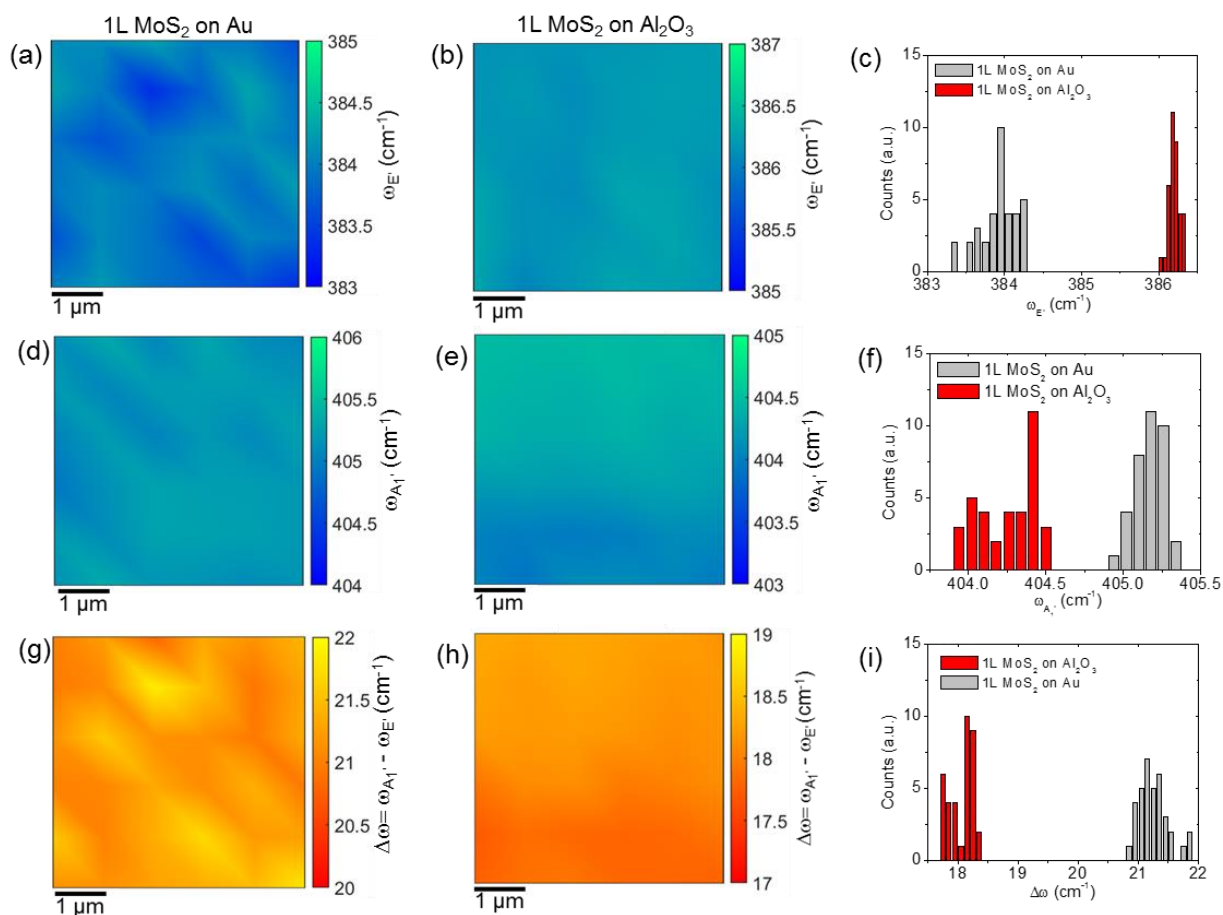


Fig.5 Colour map of the E' peak frequency values ($\omega_{E'}$) for 1L MoS₂ on Au (a) and on Al₂O₃ (b) and corresponding histograms (c). Colour map of the A₁' peak frequency values ($\omega_{A_1'}$) for 1L MoS₂ on Au (d) and on Al₂O₃ (e) and corresponding histograms (f). Colour map of the peaks frequency difference ($\Delta\omega = \omega_{A_1'} - \omega_{E'}$) for 1L MoS₂ on Au (g) and on Al₂O₃ (h) and corresponding histograms (i).

In order to extract relevant statistical information on the doping and strain uniformity of the 1L MoS₂ membranes exfoliated on Au and transferred to the Al₂O₃/Si substrate, Raman mapping was carried out on both samples by collecting arrays of 6×6 spectra on a 5×5 μm² area. Fig.5(a) and (b) show the colour maps of the E' peak frequency ($\omega_{E'}$) in the scanned areas for 1L MoS₂ on Au and Al₂O₃, respectively, while the comparison between the histograms of the $\omega_{E'}$ values in the two maps is shown in Fig.5(c). Similarly, the colour maps of the A₁' peak frequency ($\omega_{A_1'}$) and corresponding histograms are reported in Fig.5(d), (e) and (f). Beside the individual peak positions, also their difference $\Delta\omega = \omega_{A_1'} - \omega_{E'}$ was calculated for all the collected Raman spectra. The colour maps of the $\Delta\omega$ values for 1L MoS₂ on Au and Al₂O₃ are shown in Fig.5(g)-(h), and the histograms of the $\Delta\omega$ values are reported in Fig.5(i).

The comparison between the colour maps allows to visualize the spatial distribution of the $\omega_{E'}$, $\omega_{A_1'}$ and $\Delta\omega$ spectral features in the two different samples. As an example, it can be clearly deduced that the maxima of $\Delta\omega$ for the Au-supported 1L MoS₂ sample (Fig.5(g)) are correlated to the minima of the $\omega_{E'}$ map (Fig.5(a)), where the E' peak is more red-shifted. On the other hand, for the 1L MoS₂ on Al₂O₃, the $\Delta\omega$ map exhibits an almost uniform contrast, and the spatial variations are clearly correlated with those of the A₁' peak.

The histograms in Fig.5(c) and (f) confirm on a large set of data the red-shift of the E' peak and the blue-shift of the A₁' peak for 1L MoS₂ on Au with respect to 1L MoS₂ on Al₂O₃. It is also interesting to observe a significantly narrower spread of E' values for the 1L MoS₂ transferred to Al₂O₃, which can be ascribed to a more uniform strain distribution. By Gaussian fitting of the histograms, the average values and standard deviations of the peak frequencies and their difference have been obtained and reported in Table I

	$\omega_{E'} \text{ (cm}^{-1}\text{)}$	$\omega_{A_1'} \text{ (cm}^{-1}\text{)}$	$\Delta\omega \text{ (cm}^{-1}\text{)}$	$\varepsilon \text{ (}\%\text{)}$	$n \text{ (}10^{13} \text{ cm}^{-2}\text{)}$
1L MoS₂ on Au	383.9±0.3	405.1±0.1	21.2±0.3	0.21±0.06	-0.25±0.06
1L MoS₂ on Al₂O₃	386.2±0.1	404.2±0.1	18.1±0.2	-0.25±0.01	0.5±0.09

Table I Average values and standard deviation of the E', A₁' peaks frequencies ($\omega_{E'}$ and $\omega_{A_1'}$) and their difference ($\Delta\omega$), and of the evaluated strain and doping for 1L MoS₂ on Au and on Al₂O₃.

In the following, the spatial distribution of strain ε (%) and doping n (cm⁻²) for 1L MoS₂ on Au and on Al₂O₃ will be quantitatively evaluated from a correlative plot of the A₁' vs E' peak frequencies for all the Raman spectra in the maps of Fig.5. A similar approach, based on the correlative plot of the

characteristic 2D and G peaks, has been widely employed for strain and doping quantification of monolayer graphene on different substrates [39,40,41,42,43]. More recently such method has been adopted by some authors also for 1L MoS₂ [33,34,44].

In Fig.6(a), the black open circles represent the A₁' vs E' pairs for all the Raman spectra collected on 1L MoS₂ on Au, while the blue open triangles represent the data pairs for 1L MoS₂ on Al₂O₃. The red and black lines represent the theoretical relations between the frequencies of the two vibrational modes at a laser wavelength of 532 nm in the ideal cases of a purely strained (strain line) and of a purely doped (doping line) 1L MoS₂ [36,38]. The strain and doping lines cross in a point, corresponding to the $\omega_{E'}^0$ and $\omega_{A_1'}^0$, frequencies for ideally unstrained and undoped 1L MoS₂. In the following, the literature values of the peak frequencies for a suspended MoS₂ membrane ($\omega_{E'}^0 = 385 \text{ cm}^{-1}$ and $\omega_{A_1'}^0 = 405 \text{ cm}^{-1}$) [36] have been kept as the best approximation to these ideal values, as substrate effects are excluded in this case. Starting from this reference point, the directions of increasing tensile strain and n-type doping are also indicated by the arrows along the two lines.

The ε and n values for each experimental point in Fig.6(a) can be evaluated from the combination of the linear relationships between the biaxial strain/charge doping and Raman shifts of the vibrational modes:

$$\omega_{E'} = \omega_{E'}^0 - 2\gamma_{E'}\omega_{E'}^0\varepsilon + k_{E'}n \quad (1a)$$

$$\omega_{A_1'} = \omega_{A_1'}^0 - 2\gamma_{A_1'}\omega_{A_1'}^0\varepsilon + k_{A_1'}n \quad (1b)$$

Here, $\gamma_{E'}=0.68$ and $\gamma_{A_1'}=0.21$ are the Grüneisen parameters for the two vibrational modes of 1L MoS₂ [36,45,46]. The $k_{E'} = -0.33 \times 10^{-13} \text{ cm}$ and $k_{A_1'} = -2.2 \times 10^{-13} \text{ cm}$ coefficients are the shift rates of Raman peaks as a function of the electron concentration n (in cm^{-2}) in 1L MoS₂, obtained by Raman characterization of electrochemically top-gated MoS₂ transistors [38].

In particular, the relation for the strain line can be obtained by solving the system of Eqs (1a)-(1b) in the case of $n=0$:

$$\omega_{A_1'} = \omega_{A_1'}^0 + \frac{\gamma_{A_1'}\omega_{A_1'}^0}{\gamma_{E'}\omega_{E'}^0} (\omega_{E'} - \omega_{E'}^0) \quad (2)$$

whereas the doping line equation is obtained by the same procedure for $\varepsilon=0$:

$$\omega_{A_1'} = \omega_{A_1'}^0 + \frac{k_{A_1'}}{k_{E'}} (\omega_{E'} - \omega_{E'}^0) \quad (3)$$

Hence, $\frac{\gamma_{A_1'} \omega_{A_1'}^0}{\gamma_{E'} \omega_{E'}^0} = 0.32$ and $\frac{k_{A_1'}}{k_{E'}} = 6.67$ are the slopes for the strain and doping lines, respectively.

The dashed red lines parallel to the strain line ($n=0$) and the dashed black lines parallel to the doping line ($\varepsilon=0$) serve as guides to quantify the doping and strain values, respectively. They correspond to $\pm 0.1\%$ variations for the strain and $\pm 0.1 \times 10^{13} \text{ cm}^{-2}$ variations for the doping. Since the $\omega_{E'}$ is more sensitive to biaxial strain [36], the spacing between the dashed black lines parallel to the doping line is calculated from the E' mode strain rate $2\gamma_{E'} \omega_{E'}^0 = 5.2 \text{ cm}^{-1}/\%$. On the other hand, since the A_1' mode results mainly influenced by charge doping [36], the spacing between the dashed red lines parallel to the strain line is calculated from the A_1' doping rate $k_{A_1'} = 0.22 \times 10^{13} \text{ cm}$.

The plot in Fig.6(a) shows that all the experimental data points for 1L MoS₂ on Au are located above the strain line and in the left side with respect to the doping line. Hence, as compared to the reference case of a free-standing (suspended) 1L MoS₂, our gold-supported 1L MoS₂ films exhibit a tensile strain in the range from $\sim 0.1\%$ to $\sim 0.3\%$ and a p-type doping in the range from $\sim 0.1 \times 10^{13}$ to $\sim 0.4 \times 10^{13} \text{ cm}^{-2}$. The average values of the strain ($\sim 0.21\%$) and doping ($\sim 0.25 \times 10^{13} \text{ cm}^{-2}$) are indicated by the black square in Fig.6(a). A tensile biaxial strain, originating from the lattice mismatch between MoS₂ and Au [47,48], has been recently observed in the case of 1L MoS₂ exfoliated on Au also by other authors [27], that reported very large ε values up to 1.2%. The smaller tensile strain obtained in our samples are probably due to the very smooth surface of the gold films. The observed p-type doping of MoS₂ in contact with Au is consistent with several recent reports of a p-type behavior induced by MoS₂ functionalization with gold nanoparticles, adsorbates or Au-based chemicals [49,50,51].

On the other hand, the cloud of data for 1L MoS₂ on Al₂O₃ is located in a region of the ε - n plane corresponding to a compressively strained and n-type doped film, with the strain values comprised in a narrow range around $\sim -0.25\%$ and the electron density ranging from $\sim 0.4 \times 10^{13}$ to $\sim 0.7 \times 10^{13} \text{ cm}^{-2}$. The compressive strain can be plausibly related to the transfer procedure and the adhesion properties of 1L-MoS₂ with the Al₂O₃ surface. The observed n-type doping is consistent with the unintentional doping typically observed for MoS₂ layer on insulating substrates, and can be ascribed, in part, to charge transfer by adsorbed or interface trapped charges under ambient conditions, as well as to native defects of MoS₂.

By solving Eq.(1a) and (1b) for all the data points of the $\omega_{E'}$ and $\omega_{A_1'}$ maps, the corresponding colour maps of the strain (Fig.6(b)-(c)) and doping (Fig.6(e)-(f)) for the two samples were obtained. The corresponding histograms of the strain and doping values are reported in Fig.6(d) and (g), respectively. From the comparison of the strain and doping maps on the 1L MoS₂/Au, a correlation

between the regions with higher tensile strain and those with higher p-type doping can be noticed. This suggests that both strain and p-type doping originate from a locally stronger interaction with Au. On the other hand, the compressive strain distribution appears very uniform in the 1L MoS₂ membrane transferred onto Al₂O₃, without any clear correlation with the doping distribution. The average values and standard deviation of the strain and doping for the two different samples have been extracted by Gaussian fitting of the histograms in Fig.6(d) and (g), and the obtained values have been reported in the Table I. Obviously, the spatial resolution in these maps is limited by the laser spot size (~1 μm). Furthermore, the concentration sensitivity (in the order of 10¹² cm⁻²) is limited by the shift rate of the A₁' peak with doping concentration. Higher spatial resolution and sensitivity information on the doping distribution in the Au supported 1L MoS₂ will be deduced from conductive atomic force microscopy analyses reported later on in this paper.

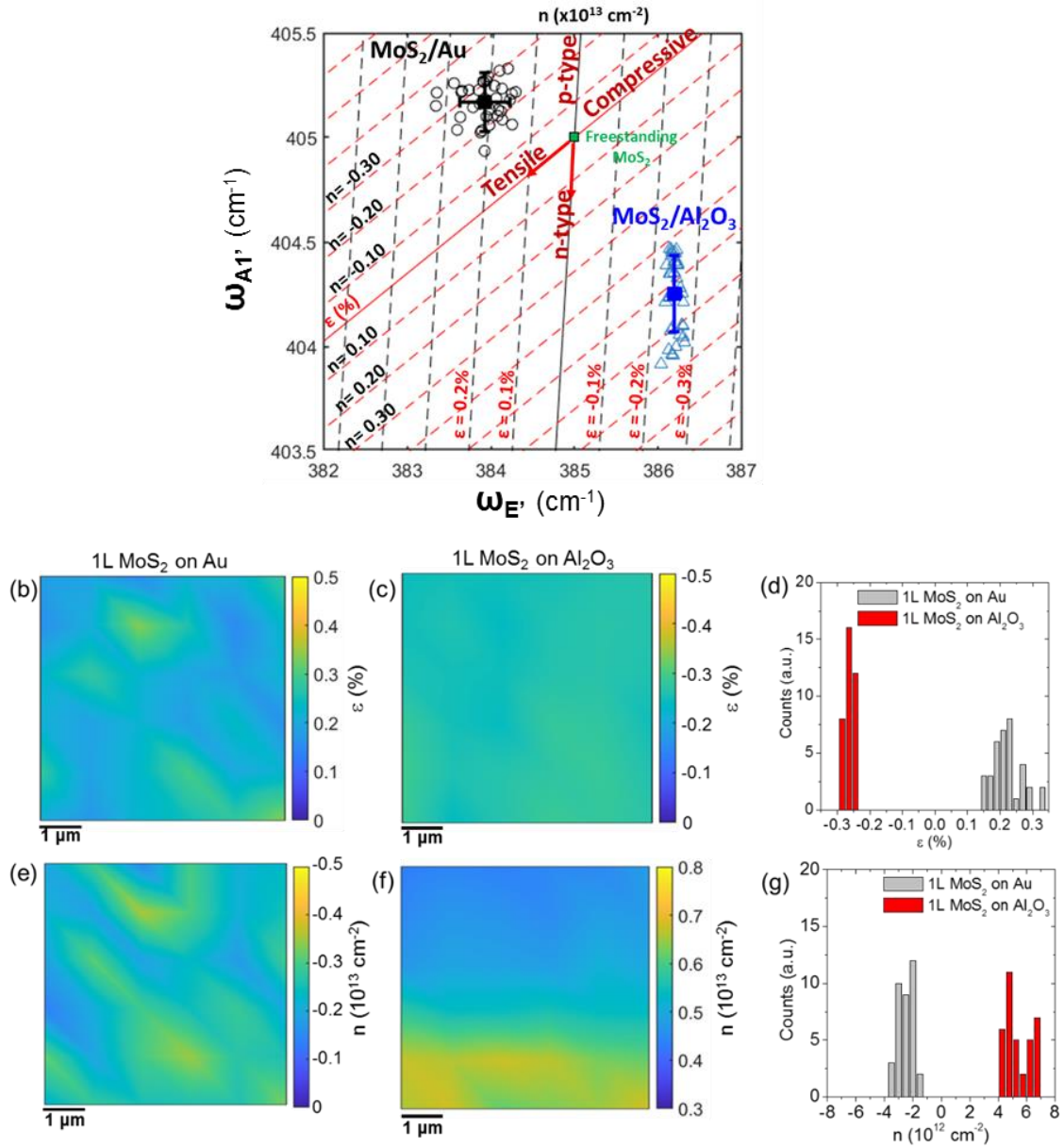


Fig.6. (a) Correlative plot of the $A_{1'}$ and E' peak frequencies to evaluate the biaxial strain and charge doping distributions in 1L MoS₂ on Au (black circles) and on Al₂O₃ (blue triangles). The red (black) lines represent the strain (doping) lines for ideally undoped (unstrained) 1L MoS₂, meanwhile the green square indicates the $\omega_{E'}^0 = 385 \text{ cm}^{-1}$ and $\omega_{A_{1'}}^0 = 405 \text{ cm}^{-1}$ frequencies for freestanding 1L MoS₂, taken as zero reference. The dashed red (black) lines parallel to the strain (doping) lines serve as guides to quantify the doping and strain values, respectively. Colour maps of the strain for the 1L MoS₂ on Au (b) and 1L MoS₂ on Al₂O₃ (c) samples and histograms of the strain values (d). Colour maps of the doping for 1L MoS₂ on Au (e) and 1L MoS₂ on Al₂O₃ (f) and histograms of the doping values (g).

To further investigate the impact of the substrate/MoS₂ interaction on the electronic properties of 1L MoS₂, micro-photoluminescence analyses were also performed using the 532 nm laser probe of the Raman equipment as excitation source. Fig.7 shows the comparison between two representative PL spectra collected on the two different samples under the same illumination conditions. Noteworthy,

the large 1L MoS₂ membrane produced by gold-assisted exfoliation and finally transferred onto Al₂O₃ exhibits a prominent peak at 1.83 eV, very similar to that observed in monolayer MoS₂ obtained by the traditional mechanical exfoliation or deposited by CVD. On the other hand, a strongly reduced PL intensity was observed when the exfoliated 1L MoS₂ membrane is still in contact with Au, together with a red-shift of the main PL peak to 1.79 eV. Such red shift has been also confirmed by comparison of arrays of PL spectra collected on the two samples, as reported in the colour maps in Fig.S4 of Supporting Information. The strong reduction of the PL intensity is consistent with the emission quenching reported by other authors for 1L MoS₂ exfoliated on Au [24] and for MoS₂ functionalized with Au nanoparticles [52]. This PL quenching can be explained in terms of a preferential transfer of photo-excited charges from MoS₂ to Au. In addition, the tensile strain of the MoS₂ layer in contact with Au can also play a role in the reduction of the PL yield, and the observed ~40 meV red shift of the main PL peak is consistent with the measured strain variation of $\Delta\epsilon\approx 0.4\%$ between the two samples [36].

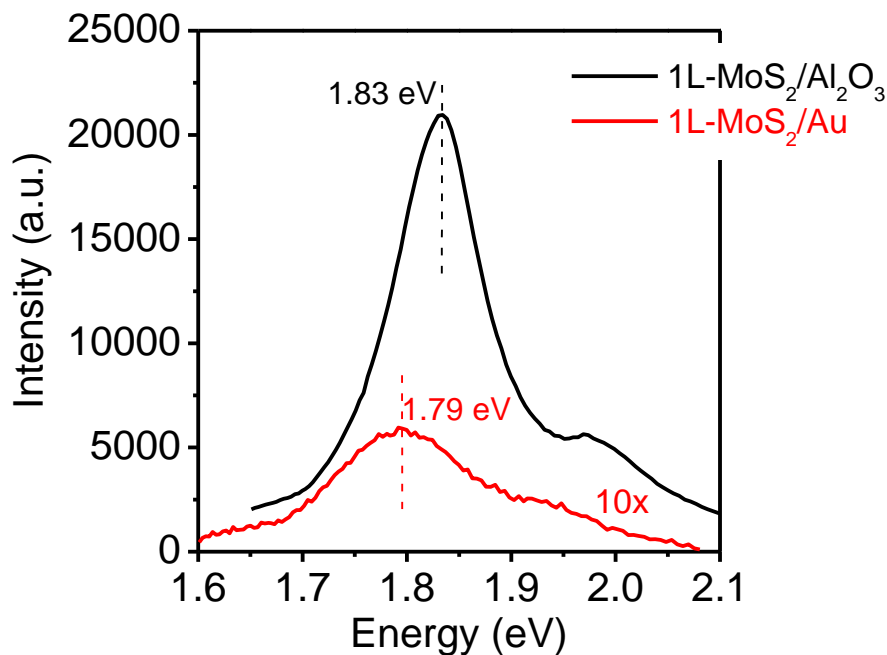


Fig.7. Typical microPL spectra collected under excitation at 532 nm on 1L MoS₂ on Au (with the intensity multiplied by a factor of 10) and 1L MoS₂ transferred to Al₂O₃.

Then, a nanoscale resolution electrical characterization of the Au-supported 1L MoS₂ membrane by C-AFM measurements [53] was carried out to get further information on the doping uniformity in this ultra-thin layer. To this aim, the current injection at the interface between the Au substrate and 1L MoS₂ was probed at nanoscale by a Pt-coated Si tip, according to the configuration schematically illustrated in Fig.8(a). The surface morphology in a sample region partially covered by 1L MoS₂ is

reported in Fig.8(b). The distribution of height values extracted from this map (Fig.8(c)) shows two components, associated to the bare Au surface and 1L MoS₂ on Au, respectively, that were fitted by Gaussian peaks with nearly identical full width at-half-maximum. This confirms how the 1L MoS₂ membrane conformally follows the smooth Au morphology. Furthermore, Fig.8(c) shows the simultaneously measured current map, collected applying a DC bias $V_{\text{tip}}=50$ mV between the Pt tip and the Au electrode (substrate). For this low bias value, the current level measured on the bare Au region reaches the current amplifier saturation limit, whereas appreciable lateral variations of the injected current through the 1L MoS₂ membrane can be observed.

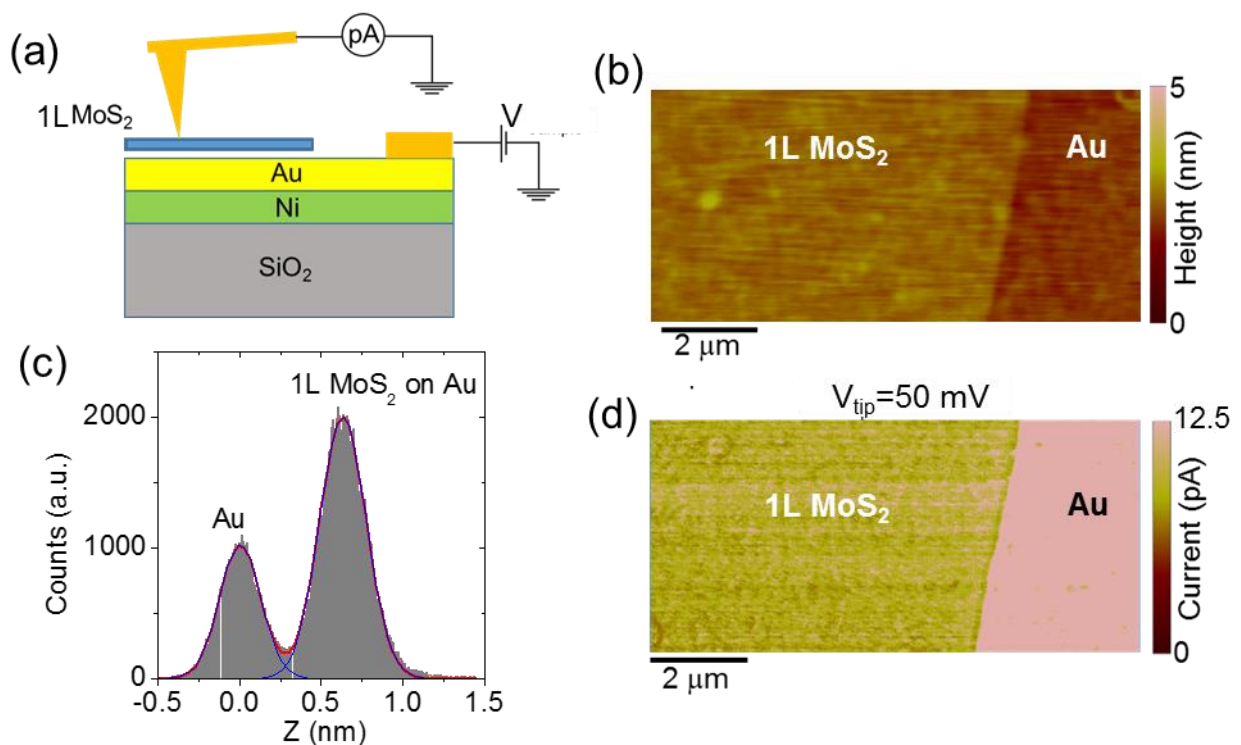


Fig.8 (a) Schematic illustration of the C-AFM setup used for current mapping through the 1L MoS₂ film on Au. (b) Morphology and (c) histogram of height distribution on a sample region with the Au substrate partially covered by the 1L MoS₂ film. (d) Simultaneously measured current map on the same area (at $V_{\text{tip}}=50$ mV).

Such local variations of the injected current through the atomically thin membrane can be ascribed to the lateral inhomogeneities of electronic properties. To further investigate this aspect and the current transport mechanisms, a set of local current-voltage (I - V_{tip}) characteristics were acquired both on the bare Au surface and at different positions on the MoS₂ film, as reported in Fig.9(a).

I - V_{tip} curves measured by the Pt tip in contact with Au (see red curve in Fig.9(a)) are very reproducible and exhibit an Ohmic behaviour with a very steep slope and current saturation at few mV positive and negative bias (as shown in the insert of Fig.9(a)). On the other hand, the curves measured on MoS₂ show a linear behaviour around $V_{\text{tip}}=0$ V with significant variations in the slope at different

positions. The slight asymmetry of the I - V_{tip} curves between positive and negative polarizations at larger bias can be ascribed to the different workfunctions of Pt and Au metals.

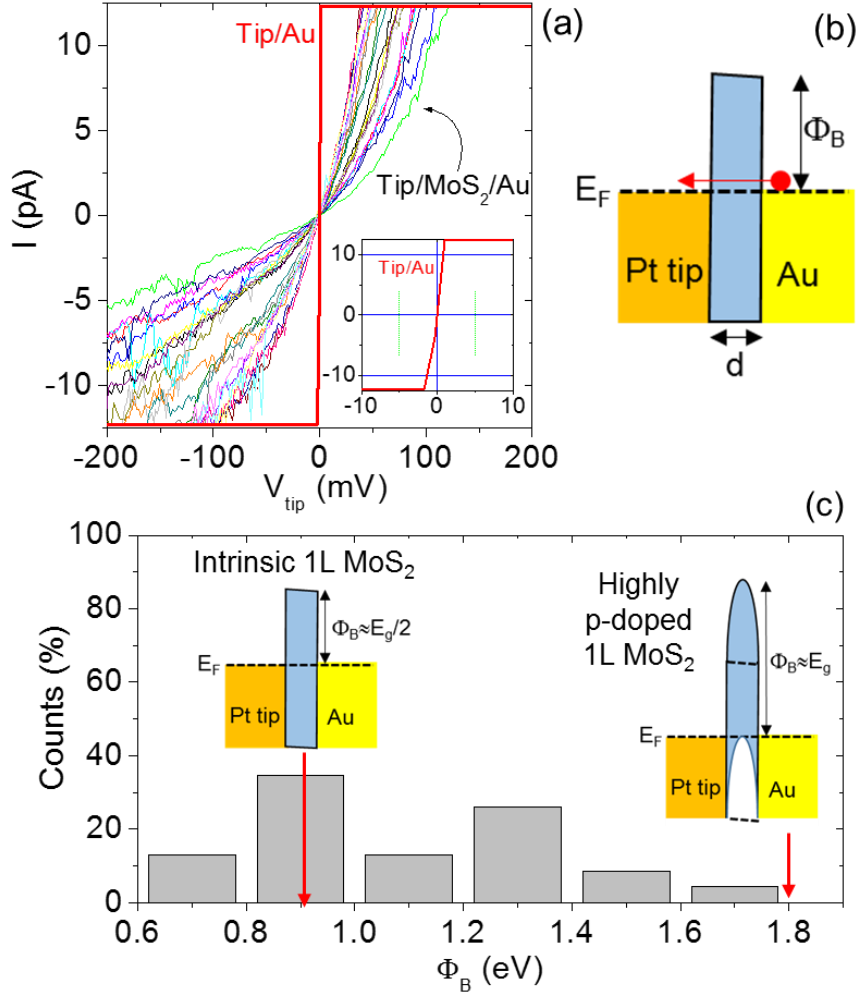


Fig.9 (a) Local I - V_{tip} curves measured with the Pt-tip in contact with 1L MoS₂ on Au and with the bare Au surface (red line). A detail of the I - V_{tip} curve measured on Au is reported in the inset. (b) Schematic band-diagram for the tip/1L MoS₂/Au metal/semiconductor/metal heterojunction. (c) Histogram of the tunnelling barrier values Φ_B evaluated from the I - V_{tip} curves in panel (a), according to the direct tunnelling mechanism. The band-diagram for intrinsic and highly p-type doped 1L MoS₂ are schematically illustrated in the inserts of (c).

The system formed by the tip in contact with the 1L MoS₂/Au can be described as a metal/semiconductor/metal heterojunction. The linear behaviour of the I - V_{tip} characteristics indicates direct tunnelling (DT) as the most appropriate mechanism ruling current transport in this heterostructure. In particular, the tunnelling current can be expressed as:

$$I_{DT} = BV_{tip} \times P(\Phi_B, d) = BV_{tip} \exp\left[-\frac{4\pi\sqrt{2m_{eff}\Phi_B}d}{h}\right] \quad (4)$$

where B is a pre-factor (proportional to the tip contact area) and $P(\Phi_B, d)$ is the direct tunnelling probability, which is a function of the tunnelling barrier thickness d (i.e. the MoS₂ thickness) and its height Φ_B , corresponding to the energy difference between the MoS₂ conduction band and the Au Fermi level (see schematic in Fig.9(b)). Here $m_{\text{eff}}=0.35 m_0$ is the electron effective mass in the transversal direction for 1L MoS₂ [54] and h is the Planck's constant. As a matter of fact, the thickness dependent tunnelling probability becomes unity when the MoS₂ layer is absent ($d=0$), i.e. when the tip is directly in contact with the Au substrate. Since current mapping and local I-V measurements have been performed using the same tip in a sample area including MoS₂-covered and uncovered Au regions, the same value for the pre-factor B were considered in the two cases. Hence, the experimental values of the local tunnelling probability at different positions on MoS₂ were estimated as the ratio between the slope of the I-V curves measured on MoS₂ and the slope of the I-V characteristics measured on Au. Since the MoS₂ layer is very conformal to the smooth Au morphology, we have assumed a laterally uniform 1L MoS₂ barrier thickness $d=0.65$ nm (corresponding to the ideal value for 1L MoS₂) over the C-AFM probed area. As a result, the local barrier height values have been extracted from the tunnelling probabilities for each of the I-V curves in Fig.9(a). The obtained histogram of the Φ_B values, reported in Fig.9(c), shows a broad distribution, extending from $\sim 0.70 \pm 0.08$ to $\sim 1.70 \pm 0.08$ eV. In particular, the component at $\Phi_B \approx 0.9$ eV in this distribution corresponds to a Fermi level located approximately at $E_g/2$ with respect to the MoS₂ conduction band, as schematically illustrated in the left insert of Fig.9(c). Noteworthy, this value is very close to ideal barrier height between Au and undoped MoS₂, given by $\Phi_B = W - \chi$, being $W \approx 5.1$ eV the gold work function and $\chi \approx 4.2$ eV the electron affinity of 1L MoS₂ [55]. On the other hand, the tail at larger Φ_B values in the distribution of Fig.9(c) can be ascribed to the local p-type doping (i.e., the upward bending of the valence and conduction bands) of 1L-MoS₂ induced by the Au substrate. In particular, in the regions with the highest p-type doping, the barrier height approaches the value of the bandgap ($\Phi_B \approx E_g$), as schematically illustrated in the right insert of Fig.9(c). Hence, the C-AFM characterization reveals variations in the local p-type doping of the Au-supported 1L MoS₂ membrane over a broad range.

Finally, the electronic transport in 1L MoS₂ membrane transferred onto the Al₂O₃ dielectric surface has been investigated by electrical characterization of a field effect transistor (FET) with the Al₂O₃ (100 nm)/Si back-gate and Au source and drain contacts (channel length $L=10$ μm), as illustrated in the insert of Fig.10(a). The output characteristics (drain current vs drain bias, $I_D - V_D$) of the device for different gate bias values ranging from $V_G = -20$ to 10 V are shown in Fig.10(a). At low drain bias ($V_D < 3$ V) current injection in the MoS₂ channel is limited by the high Schottky barrier at Au/MoS₂ contacts, whereas a linear behaviour of the $I_D - V_D$ characteristics is observed at intermediate V_D values

(from 3 to 10 V), followed by current saturation at higher voltages. The transfer characteristic (I_D - V_G) at a drain bias $V_D=5V$ (i.e. in the linear region of I_D - V_D curves) is reported in Fig.10(b), black line. The monotonic increase of I_D with V_G is the typically observed behaviour for a transistor with an n-type MoS₂ channel. A negative threshold voltage $V_{th}\approx-8$ V was evaluated by linear fitting of the I_D - V_G curve and taking the intercept with the voltage axis, as indicated by the arrow in Fig.10(b). Since V_{th} represents the bias necessary to deplete the n-type MoS₂ channel, the electron density can be estimated as $n=C_{ox}|V_{th}|/q$, where $C_{ox}=\epsilon_0\epsilon_{ox}/t$ is the Al₂O₃ capacitance per unit area, with ϵ_0 the vacuum permittivity and $\epsilon_{ox}=8$ is the relative dielectric constant of the Al₂O₃ dielectric. The obtained carrier density $n\approx 3.1\times 10^{12}$ cm⁻² is in reasonably good agreement with the carrier density values obtained by Raman mapping.

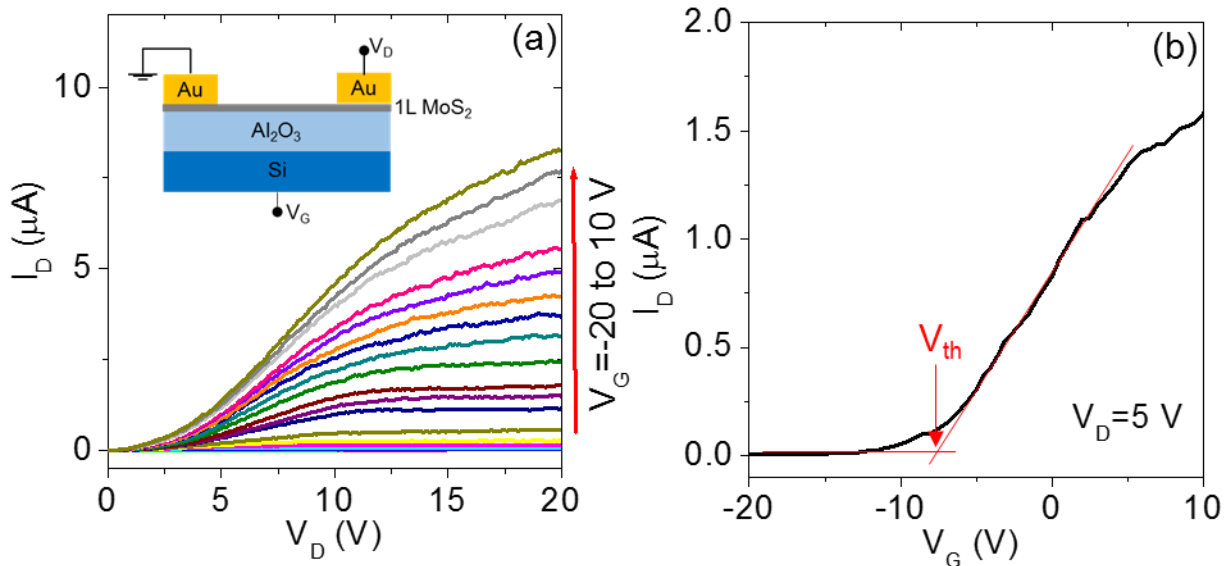


Fig.10 (a) Output and (b) transfer characteristics of a back-gated field effect transistor fabricated with Au-exfoliated 1L MoS₂ transferred on Al₂O₃/Si. The device schematic is shown in the insert of panel (a).

Hence, also this device-level characterization confirmed that the large area 1L MoS₂ films produced by Au-assisted exfoliation, after the final transfer to an insulating substrate and complete removal of gold, recover the same electrical properties of the MoS₂ flakes produced by the conventional mechanical exfoliation or by chemical vapour deposition.

Conclusion

In summary, large area (cm^2) 1L MoS₂ membranes have been exfoliated on very flat gold films and transferred to an insulating Al₂O₃/Si substrate. For 1L MoS₂ in contact with Au, Raman mapping revealed a spatially inhomogeneous distribution of tensile strain (in the range from $\sim 0.1\%$ to $\sim 0.3\%$) and p-type doping (from $\sim 0.1 \times 10^{13}$ to $\sim 0.4 \times 10^{13} \text{ cm}^{-2}$), with a correlation between regions showing higher strain and doping. The electrical properties of Au-supported MoS₂ were probed at nanoscale by C-AFM, showing direct tunnelling across the ultra-thin 1L-MoS₂, with a broad distribution of tunnelling barrier values (Φ_B from 0.7 to 1.7 eV) consistent with an inhomogeneous p-type doping of MoS₂. After the final transfer of 1L MoS₂ on Al₂O₃/Si, the strain was converted to compressive ($\epsilon \approx 0.25\%$) with a very uniform distribution. Furthermore, an n-type doping ($n \approx 0.5 \times 10^{13} \text{ cm}^{-2}$) was deduced by Raman and confirmed by electrical measurements of an Al₂O₃/Si back-gated 1L MoS₂ transistor. These results provide a deeper understanding of the properties of large area 1L MoS₂ produced by Au-assisted exfoliation, and will contribute to the widespread application of this outstanding quality material in the demonstration of novel device concept and synthetic Van der Waals heterostructures.

Materials and Methods

Samples preparation. The deposition of Ni(10 nm)/Au (15 nm) on the SiO₂(900 nm)/Si sample was carried out by DC magnetron sputtering using a Quorum equipment. The base vacuum in the chamber was $\sim 10^{-5}$ mbar, meanwhile during the deposition process the pressure was of about 10^{-4} - 10^{-3} mbar. The same equipment was employed to deposit 100 nm Au on a Si sample for the preparation of the gold tape with the peeling technique (see Fig.2). PMMA (200K, 0.5 μm) was spin coated on Au and tempered at 150°C. A Nitto Denko thermal release tape (with 120 °C release temperature) was used for the handling of the PMMA/Au gold tape. The 100 nm Al₂O₃ insulator on Si (used as a final substrate for 1L MoS₂ transfer) was deposited by DC-pulsed RF reactive sputter.

AFM and CAFM analyses. Morphological analyses of the Au/Ni substrates and of the exfoliated MoS₂ films were carried out by tapping mode Atomic Force Microscopy (AFM) using a DI3100 equipment by Bruker with Nanoscope V electronics. Sharp silicon tips with a curvature radius of 5 nm were used for these measurements. C-AFM measurements were carried out with the same AFM system equipped with the TUNA module and using Pt coated Si tips.

Micro-Raman and micro-Photoluminescence. Raman spectroscopy and PL measurements were carried out using a Horiba HR-Evolution micro-Raman system with a confocal microscope (100 \times objective) and a laser excitation wavelength of 532 nm. The laser power used for these analyses was

filtered with a neutral density filter at 1% ensuring no sample degradation. A grating of 1800 lines/mm was employed to acquire Raman spectra in a range from 150 to 650 cm^{-1} , while a grating of 600 lines/mm was used to acquire Photoluminescence spectra in a range from 10 to 5500 cm^{-1} . All the spectra were calibrated with respect to the Silicon peak at 520.7 cm^{-1} .

Field effect transistor preparation and characterization: A back-gated 1L MoS₂ field effect transistor was fabricated with the Au-exfoliated film transferred onto Al₂O₃ (100 nm)/Si by sputtering Au source/drain contacts with a shadow mask. The contact spacing, i.e. the channel length was L=10 μm . The output and transfer characteristics of the transistor were measured in dark conditions using a Cascade Microtech probe station with an Agilent 4156b parameter analyzer.

Acknowledgements

The authors acknowledge S. Di Franco (CNR-IMM) for the assistance in the samples preparation, P. Fiorenza and R. Lo Nigro (CNR-IMM) and M. Cannas (Univ. of Palermo) for useful discussions. The paper has been supported, in part, by MUR in the framework of the FlagERA-JTC 2019 project "ETMOS". E.S. acknowledges the PON project EleGaN_{Te} (ARS01_01007) for financial support. Part of the experiments have been carried out using the facilities of the Italian Infrastructure Beyond Nano.

References

-
- ¹ Wang, Q. H.; Zadeh, K. K.; Kis, A.; Coleman, J. N.; Strano, M. S. Electronics and optoelectronics of two-dimensional transition metal dichalcogenides. *Nat. Nanotechnol.* **2012**, *7*, 699.
 - ² Radisavljevic, B; Whitwick, M. B.; Kis., A. Integrated circuits and logic operations based on single-layer MoS₂. *ACS Nano* **2011**, *5* (12), 9934-9938.
 - ³ Lopez-Sanchez, O.; Lembke, D.; Kayci, M.; Radenovic, A.; Kis, A. Ultrasensitive photodetectors based on monolayer MoS₂. *Nature nanotechnology* **2013**, *8* (7), 497-501.
 - ⁴ Yin, Z.; Li, H.; Li, Ho.; Jiang, L.; Shi, Y.; Sun, Y.; Lu, G.; Zhang, Q.; Chen, X.; Zhang, H. Single-layer MoS₂ phototransistors. *ACS nano* **2012**, *6* (1), 74-80.
 - ⁵ Li, H.; Yin, Z.; He, Q.; Li, H.; Huang, X.; Lu, G.; Fam, D.W.H.; Tok, A.I.Y.; Zhang, Q; Zhang, H. Fabrication of single-and multilayer MoS₂ film-based field-effect transistors for sensing NO at room temperature. *Small* **2012** *8* (1), 63-67.
 - ⁶ Kuc, A.; Zibouche, N.; Heine, T. Influence of quantum confinement on the electronic structure of the transition metal sulfide TS₂. *Physical Review B* **2011**, *83* (24), 245213.

-
- ⁷ Wilson, J.A.; Yoffe, A. D. The transition metal dichalcogenides discussion and interpretation of the observed optical, electrical and structural properties. *Advances in Physics* **1969**, 18 (73), 193-335.
- ⁸ Mak, K.F.; Hone, Lee, C.; Hone, J.; Shan, J.; Heinz, T.F. Atomically thin MoS₂: a new direct-gap semiconductor. *Physical review letters* **2010**, 105 (13), 136805.
- ⁹ Velický, M.; Toth, P.S. From two-dimensional materials to their heterostructures: An electrochemist's perspective. *Applied Materials Today* **2017**, 8, 68-103.
- ¹⁰ Splendiani, A.; Sun, L.; Zhang, Y.; Li, T.; Kim, J.; Chim, C.-Y.; Galli, G.; Wang, F. Emerging photoluminescence in monolayer MoS₂. *Nano letters* **2010**, 10 (4), 1271-1275.
- ¹¹ Ayari, A.; Cobas, E.; Ogundadegbe, O.; Fuhrer, M.S. Realization and electrical characterization of ultrathin crystals of layered transition-metal dichalcogenides. *Journal of applied physics* **2007**, 101 (1), 014507.
- ¹² Yoon, Y.; Ganapathi, K.; Salahuddin, S. How good can monolayer MoS₂ transistors be?. *Nano letters* **2011**, 11 (9), 3768-3773.
- ¹³ Radisavljevic, B.; Radenovic, A.; Brivio, J.; Giacometti, V.; Kis, A. Single-layer MoS₂ transistors. *Nature nanotechnology* **2011**, 6 (3), 147-150.
- ¹⁴ Tosun, M.; Fu, D.; Desai, S. B.; Ko, C.; Kang, J. S.; Lien, D.-H.; Najmzadeh, M.; Tongay, S.; Wu, J.; Javey, A. MoS₂ Heterojunctions by Thickness Modulation, *Scientific Reports* **2015**, 5, 10990.
- ¹⁵ Conley, H.J.; Wang, B.; Ziegler, J.I.; Haglund, Jr. R.F.; Pantelides, S.T.; Bolotin, K.I. Bandgap Engineering of Strained Monolayer and Bilayer MoS₂, *Nano Lett.* **2013**, 13 (8), 3626–3630.
- ¹⁶ Giannazzo, F. Engineering 2D heterojunctions with dielectrics. *Nat. Electron.* **2019**, 2, 54–55.
- ¹⁷ Giannazzo, F.; Greco, G.; Roccaforte, F.; Sonde, S.S. Vertical Transistors Based on 2D Materials: Status and Prospects. *Crystals* **2018**, 8 (2), 70.
- ¹⁸ Lee, Y.H.; Zhang, X.-Q.; Zhang, W.; Chang, M.-T.; Lin, C.-T.; Chang, K.-D.; Yu, Y.-C.; Wang, J.T.-W.; Chang, C.-S.; Li, L.-J.; Lin, T.-W. Synthesis of large-area MoS₂ atomic layers with chemical vapor deposition. *Advanced materials* **2012**, 24 (17), 2320-2325.
- ¹⁹ Zhan, Y.; Liu, Z.; Najmaei, S.; Ajayan, P.M.; Lou, J. Large-area vapor-phase growth and characterization of MoS₂ atomic layers on a SiO₂ substrate. *Small* **2012**, 8 (7), 966-971.
- ²⁰ Fu, D.; Zhao, X.; Zhang, Y.-Y.; Li, L.; Xu, H.; Jang, A.-R.; Yoon, S. I.; Song, P.; Poh, S. M.; R., Tianhua; Ding, Z.; Fu, W.; Shin, T. J.; Shin, H. S.; Pantelides, S. T.; Zhou, W.; Loh, K. P. Molecular Beam Epitaxy of Highly Crystalline Monolayer Molybdenum Disulfide on Hexagonal Boron Nitride, *J. Am. Chem. Soc.* **2017**, 139, 9392–9400.
- ²¹ Ho, Y.-T.; Ma, C.-H.; Luong, T.-T.; Wei, L.-L.; Yen, T.-C.; Hsu, W.-T.; Chang, W.-H.; Chu, Y.-C.; Tu, Y.-Y.; Pande, K.P.; Chang, E.Y. Layered MoS₂ grown on c-sapphire by pulsed laser deposition. *Physica Status Solidi (RRL)–Rapid Research Letters* **2015**, 9 (3), 187-191.

-
- ²² Novoselov, K.S.; Jiang, D.; Schedin, F.; Booth, T.J.; Khotkevich, V.V.; Morozov, S.V.; Geim, A.K. Two-dimensional atomic crystals. *Proceedings of the National Academy of Sciences* **2005**, *102* (30), 10451-10453.
- ²³ Lee, C.; Yan, H.; Brus, L.E.; Heinz, T.F.; Hone, J.; Ryu, S. Anomalous lattice vibrations of single- and few-layer MoS₂. *ACS nano* **2010**, *4* (5), 2695-2700.
- ²⁴ Velický, M.; Donnelly, G.E.; Hendren, W.R.; McFarland, S.; Scullion, D.; DeBenedetti, W.J.I.; Correa, G.C.; Han, Y.; Wain, A.J.; Hines, M.A.; Muller, D.A.; Novoselov, K.S.; Abruña, H.D.; Bowman, R.M.; Santos, E.J.G.; Huang, F. Mechanism of gold-assisted exfoliation of centimeter-sized transition-metal dichalcogenide monolayers. *ACS nano* **2018**, *2* (10), 10463-10472.
- ²⁵ Desai, S.B.; Madhvapathy, S.R.; Amani, M.; Kiriyama, D.; Hettick, M.; Tosun, M.; Zhou, Y.; Dubey, M.; Ager III, J.W.; Chrzan, D.; Javey, A. Gold-mediated exfoliation of ultralarge optoelectronically-perfect monolayers. *Advanced Materials* **2016**, *28* (21), 4053-4058.
- ²⁶ Magda, G.Z.; Pető, J.; Dobrik, G.; Hwang, C.; Biró, L.P.; Tapasztó, L. Exfoliation of large-area transition metal chalcogenide single layers. *Scientific reports* **2015**, *5*, 14714.
- ²⁷ Velický, M.; Rodriguez, A.; Bouša, M.; Krayev, A.V.; Vondráček, M.; Honolka, J.; Ahmadi, M.; Donnelly, G.E.; Huang, F.; Abruña, H.D.; Novoselov, K.S.; Frank, O. Strain and Charge Doping Fingerprints of the Strong Interaction between Monolayer MoS₂ and Gold. *The journal of physical chemistry letters* **2020**, *11* (15), 6112-6118.
- ²⁸ Gramling, H. M.; Towle, C. M.; Desai, S. B.; Sun, H.; Lewis, E. C.; Nguyen, V. D.; Ager, J. W.; Chrzan, D.; Yeatman, E. M.; Javey, A.; Taylor, H. Spatially Precise Transfer of Patterned Monolayer WS₂ and MoS₂ with Features Larger than 10⁴ μm² Directly from Multilayer Sources, *ACS Appl. Electron. Mater.* **2019**, *1*, 407–416.
- ²⁹ Liu, F.; Wu, W.; Bai, Y.; Chae, S. H.; Li, Q.; Wang, J.; Hone, J.; Zhu, X.-Y. Disassembling 2D van der Waals crystals into macroscopic monolayers and reassembling into artificial lattices. *Science* **2020**, *367*, 903–906.
- ³⁰ Hegner, M.; Wagner, P.; Semenza, G. Ultralarge atomically flat template-stripped Au surfaces for scanning probe microscopy. *Surf. Sci.* **1993**, *291*, 39–46.
- ³¹ Vogel, N.; Zieleniecki, J.; Köper, I. As flat as it gets: ultrasoft surfaces from template-stripping procedures. *Nanoscale* **2012**, *4*, 3820–3832
- ³² Zhan, Y.; Liu, Z.; Najmaei, S.; Ajayan, P.M.; Lou, J. Large-Area Vapor-Phase Growth and Characterization of MoS₂ Atomic Layers on a SiO₂ Substrate. *Small* **2012**, *8* (7), 966-971.
- ³³ Chae, W.H.; Cain, J.D.; Hanson, E.D. Substrate-induced strain and charge doping in CVD-grown monolayer MoS₂. *Applied Physics Letters* **2017**, *111* (14), 143106.

-
- ³⁴ Michail, A.; Delikoukos, N.; Parthenios, J.; Galiotis, C.; Papagelis, K. Optical detection of strain and doping inhomogeneities in single layer MoS₂. *Applied Physics Letters* **2016**, *108* (17), 173102.
- ³⁵ McCreary, A.; Ghosh, R.; Amani, M.; Wang, J.; Duerloo, K. A. N.; Sharma, A.; Jarvis, K.; Reed, E.J.; Dongare, A.M.; Banerjee, S.K.; Terrones, M.; Namburu, R.R.; Dubey, M. Effects of uniaxial and biaxial strain on few-layered terrace structures of MoS₂ grown by vapor transport. *ACS nano*, **2016**, *10* (3), 3186-3197.
- ³⁶ Lloyd, D.; Liu, X.; Christopher, J.W.; Cantley, L.; Wadehra, A.; Kim, B.L.; Goldberg, B.B.; Swan, A.K.; Bunch, J.S. Band gap engineering with ultralarge biaxial strains in suspended monolayer MoS₂. *Nano letters* **2016**, *16* (9), 5836-5841.
- ³⁷ Melnikova-Kominkova, Z.; Jurkova, K.; Vales, V.; Drogowska-Horná, K.; Frank, O.; Kalbac, M. Strong and efficient doping of monolayer MoS₂ by a graphene electrode. *Physical Chemistry Chemical Physics* **2019**, *21* (46), 25700-25706.
- ³⁸ Chakraborty, B.; Bera, A.; Muthu, D.V.S.; Bhowmick, S.; Waghmare, U.V.; Sood, A.K. Symmetry-dependent phonon renormalization in monolayer MoS₂ transistor. *Physical Review B* **2012**, *85* (16), 161403.
- ³⁹ Lee, J.E.; Ahn, G.; Shim, J.; Lee, Y.S.; Ryu, S. Optical separation of mechanical strain from charge doping in graphene. *Nature communications* **2012**, *3* (1), 1-8.
- ⁴⁰ Armano, A.; Buscarino, G.; Cannas, M.; Gelardi, F. M.; Giannazzo, F.; Schilirò, E.; Agnello, S. Monolayer graphene doping and strain dynamics induced by thermal treatments in controlled atmosphere. *Carbon* **2018**, *127*, 270-279.
- ⁴¹ Mohiuddin, T. M. G.; Lombardo, A.; Nair, R.R.; Bonetti, A.; Savini, G.; Jalil, R.; Bonini, N.; Basko, D.M.; Galiotis, C.; Marzari, N.; Novoselov, K.S.; Geim, A.K.; Ferrari, A.C. Uniaxial strain in graphene by Raman spectroscopy: G peak splitting, Grüneisen parameters, and sample orientation. *Physical Review B* **2009**, *79* (20), 205433.
- ⁴² Androulidakis, Ch.; Tsoukleri, G.; Koutroumanis, N.; Gkikas, G.; Pappas, P.; Parthenios, J.; Papagelis, K.; Galiotis, C. Experimentally derived axial stress–strain relations for two-dimensional materials such as monolayer graphene. *Carbon* **2015**, *81*, 322-328.
- ⁴³ Schilirò, E.; Lo Nigro, R.; Panasci, S. E.; Gelardi, F. M.; Agnello, S.; Yakimova, R.; Roccaforte F.; Giannazzo, F. Aluminum oxide nucleation in the early stages of atomic layer deposition on epitaxial graphene. *Carbon* **2020**, *169*, 172-181.
- ⁴⁴ Rao, R.; Islam, A.E.; Singh, S.; Berry, R.; Kawakami, R.K.; Maruyama, B.; Katoch, J. Spectroscopic evaluation of charge-transfer doping and strain in graphene/MoS₂ heterostructures. *Physical Review B* **2019**, *99* (19), 195401.

-
- ⁴⁵ Jorio, A.; Dresselhaus, M.S.; Saito, R.; Dresselhaus, G. Raman spectroscopy in graphene related systems. *John Wiley & Sons* **2011**.
- ⁴⁶ Ferralis, N. Probing mechanical properties of graphene with Raman spectroscopy. *Journal of materials science* **2010**, *45* (19), 5135-5149.
- ⁴⁷ Gong, C.; Huang, C.; Miller, J.; Cheng, L.; Hao, Y.; Cobden, D.; Kim, J.; Ruoff, R. S.; Wallace, R. M.; Cho, K.; et al. Metal Contacts on Physical Vapor Deposited Monolayer MoS₂. *ACS Nano* **2013**, *7*, 11350–11357.
- ⁴⁸ Sørensen, S. G.; Füchtbauer, H. G.; Tuxen, A. K.; Walton, A. S.; Lauritsen, J. V. Structure and Electronic Properties of In Situ Synthesized Single-Layer MoS₂ on a Gold Surface. *ACS Nano* **2014**, *8*, 6788–6796.
- ⁴⁹ Singh, A. K.; Pandey, R. K.; Prakash, R.; Eom, J. Tailoring the charge carrier in few layers MoS₂ field-effect transistors by Au metal adsorbate, *Appl. Surface Science* **2018**, *437*, 70–74
- ⁵⁰ Liu, H.; Grasseschi, D.; Dodda, A.; Fujisawa, K.; Olson, D.; Kahn, E.; Zhang, F.; Zhang, T.; Lei, Y.; Branco, R. B. N.; Elías, A. L.; Silva, R. C.; Yeh, Y.-T.; Maroneze, C. M.; Seixas, L.; Hopkins, P.; Das, S.; de Matos, C. J. S.; Terrones, M. Spontaneous chemical functionalization via coordination of Au single atoms on monolayer MoS₂, *Science Advances* **2020**, *6*, abc9308.
- ⁵¹ Liu, X.; Qu, D.; Ryu, J.; Ahmed, F.; Yang, Z.; Lee, D.; Yoo, W. J. P-Type Polar Transition of Chemically Doped Multilayer MoS₂ Transistor, *Adv. Mater.* **2016**, *28*, 2345–2351.
- ⁵² Bhanu, U.; Islam, M.R.; Tetard, L.; Khondaker, S.I. Photoluminescence quenching in gold-MoS₂ hybrid nanoflakes. *Scientific reports* **2014**, *4*, 5575.
- ⁵³ Giannazzo, F.; Schilirò, E.; Greco, G.; Roccaforte, F. Conductive Atomic Force Microscopy of Semiconducting Transition Metal Dichalcogenides and Heterostructures, *Nanomaterials* **2020**, *10*, 803.
- ⁵⁴ Cheiwchanamngij, T.; Lambrecht, W.R.L. Quasiparticle band structure calculation of monolayer, bilayer, and bulk MoS₂, *Phys. Rev. B* **2012**, *85*, 205302.
- ⁵⁵ Lee, H.; Deshmukh, S.; Wen, J.; Costa, V. Z.; Schuder, J. S.; Sanchez, M.; Ichimura, A. S.; Pop, E.; Wang, B.; Newaz, A. K. M. Layer-Dependent Interfacial Transport and Optoelectrical Properties of MoS₂ on Ultraflat Metals, *ACS Appl. Mater. Interfaces* **2019**, *11*, 31543–31550.